

SUPPORTING INFORMATION

Electrical Double Layer-Induced Ion Surface Accumulation for Ultrasensitive Refractive Index Sensing with Nanostructured Porous Silicon Interferometers

Stefano Mariani¹, Lucanos Marsilio Strambini², Giuseppe Barillaro^{1,2*}

¹Dipartimento di Ingegneria dell'Informazione, Università di Pisa, via G. Caruso 16, 56122 Pisa, Italy

²Istituto di Elettronica e di Ingegneria dell'Informazione e delle Telecomunicazioni, Consiglio Nazionale delle Ricerche, via G. Caruso 16, 56122 Pisa, Italy

*g.barillaro@iet.unipi.it

These *Supporting Information* provide additional details and data on: 1) calculation of refractive index values of deionized water (DIW), sodium chloride (NaCl), and potassium chloride (KCl) at wavelength and temperature values used in this work (i.e. $\lambda = 588$ nm and $T = 18^\circ\text{C}$); 2) calculation of refractive index n_{sol} and refractive index variations Δn_{sol} (with respect to DIW) values of the prepared NaCl and KCl aqueous solutions at different concentrations; 3) experimental optofluidic setup used for the refractometric characterization; 4) routine for the calculation of the IAW signal; 5) theoretical model of PSi interferometers for monitoring bulk refractive index variation of solutions infiltrating the pores using IAW reflectance spectroscopy; 6) calibration curve of PSi interferometers infiltrated with NaCl aqueous solutions at different concentrations obtained through Fast Fourier Transform (FFT) reflectance spectroscopy.

Section 1. Calculation of refractive index values of deionized water (DIW), sodium chloride (NaCl), and potassium chloride (KCl) at $\lambda = 588$ nm and $T = 18^\circ\text{C}$

The procedures used to calculate refractive index values at wavelength and temperature used in this work, namely 588 nm and 18°C , from high accuracy refractive index values available in the literature are here below detailed:

DIW refractive index at 588 nm and 18°C - M. Daimon et al.¹ measured for deionized water (DIW) a refractive index value $n_{DIW} = 1.333260$ (uncertainty ± 0.000008) RIU at $\lambda = 587.725$ nm and $T = 21.5^\circ\text{C}$. Given the wavelength derivative of DIW refractive index, namely thermo-optic coefficient $dn_{DIW}/dT = -95.3 \pm 2.2 \times 10^{-6} \text{ }^\circ\text{C}^{-1}$ at $\lambda = 587.725$ nm and $T = 21.5^\circ\text{C}$, a refractive index value $n_{DIW} = 1.333594 \pm 0.000016$ RIU is estimated at $\lambda = 587.725$ nm and $T = 18^\circ\text{C}$.

NaCl refractive index at 588 nm and 18°C - H. H. Li² measured for NaCl a refractive index $n_{NaCl} = 1.5441 \pm 0.0001$ RIU at $\lambda = 590$ nm and $T = 20^\circ\text{C}$. Given both wavelength derivative $dn_{NaCl}/d\lambda = -0.0638 \text{ } \mu\text{m}^{-1}$ and temperature derivative $dn_{NaCl}/dT = -3.2 \pm 0.2 \times 10^{-5} \text{ K}^{-1}$ of NaCl refractive index, a refractive index value $n_{NaCl} = 1.5443 \pm 0.0001$ RIU is estimated at $\lambda = 588$ nm and $T = 18^\circ\text{C}$.

KCl refractive index at 588 nm and 18°C - M. Daimon et al.¹ measured for KCl a refractive index $n_{KCl} = 1.4902 \pm 0.0001$ RIU at $\lambda = 590$ nm and $T = 20^\circ\text{C}$. Given both wavelength derivative $dn_{KCl}/d\lambda = -0.0555 \text{ } \mu\text{m}^{-1}$ and temperature derivative $dn_{KCl}/dT = -3.16 \pm 0.4 \times 10^{-5} \text{ K}^{-1}$ of KCl, a refractive index value $n_{KCl} = 1.4904 \pm 0.0001$ RIU is estimated at $\lambda = 588$ nm and $T = 18^\circ\text{C}$.

Section 2. Calculation of refractive index n_{sol} and refractive index variations Δn_{sol} (with respect to DIW) values of NaCl and KCl aqueous solutions at different concentrations

Given the composition of NaCl and KCl solutions used in this work, calculation of n_{sol} values is carried out using the Lorenz-Lorenz equation³. The uncertainty on the resulting n_{sol} value is related to uncertainties on the NaCl, KCl, and DIW refractive index values and on the volume fraction value f_i

of the prepared solutions. The formers are given in Section 1, whereas the latter are given in Tables S1 and S2 of this section (f_i calculation is described in the *Methods* section).

In order to take into account the parameters uncertainties on the calculation of n_{sol} , for each tested concentration a Monte Carlo statistical analysis is carried out under the assumption that all the physical parameters (i.e. refractive indices and volume fraction) involved in the calculation have a Gaussian distribution. A Matlab algorithm is developed to generate $N=10^6$ realizations for the calculation of n_{sol} using the Lorentz-Lorentz equation. For each realization, a random value is chosen for both NaCl (KCl) and DIW refractive indices, as well as for the volume fraction of NaCl (KCl) at the given concentration. For each tested concentration, the resulting n_{sol} values have a Gaussian distribution with mean value and standard deviation tabulated in Tables S1 and S2 for NaCl and KCl solutions, respectively. The standard deviation value of n_{sol} in Tables S1 and S2 is 1×10^{-4} RIU, which points out that the refractive index variation (with respect to DIW) $\Delta n_{sol} = n_{sol} - n_{DIW}$ is statistically significant only when its value is greater than 1×10^{-4} RIU. Therefore, the refractive index variation value Δn_{sol} in Tables S1 and S2 is calculated as the difference between n_{sol} and n_{DIW} only for

| NaCl:H ₂ O (mg/ml) | NaCl % (w/w)* | | f_{i-NaCl} (v/v) | | n_{sol} | | Δn_{sol} | |
|----------------------------------|------------------------|--------------------|------------------------|---------------------|---------------|----------------------|--|---------------------|
| | Mean | STD | Mean | STD | Mean | STD | Mean | STD |
| 0 (DIW) | 0 | / | 0 | / | 1.333594 | 1.6×10^{-5} | 0 | / |
| 1:10⁷ | 0.970×10^{-5} | 3×10^{-8} | 3.085×10^{-8} | 9×10^{-11} | / | / | 6.3×10^{-9} | 1×10^{-10} |
| 1:10⁶ | 0.970×10^{-4} | 3×10^{-7} | 3.085×10^{-7} | 9×10^{-10} | / | / | 6.3×10^{-8} | 1×10^{-9} |
| 1:10⁵ | 0.970×10^{-3} | 2×10^{-6} | 3.085×10^{-6} | 8×10^{-9} | / | / | 6.3×10^{-7} | 1×10^{-8} |
| 1:10⁴ | 0.970×10^{-2} | 2×10^{-5} | 3.085×10^{-5} | 7×10^{-8} | / | / | 6.3×10^{-6} | 1×10^{-7} |
| 1:1000 | 0.970×10^{-1} | 2×10^{-4} | 3.085×10^{-4} | 6×10^{-7} | / | / | 6.3×10^{-5} | 1×10^{-6} |
| 1:100 | 9.641×10^{-1} | 8×10^{-4} | 3.085×10^{-3} | 5×10^{-6} | 1.3342 | 1×10^{-4} | 0.604×10^{-3} | 1×10^{-6} |
| 1:50 | 1.963 | 1×10^{-3} | 5.925×10^{-3} | 8×10^{-6} | 1.3347 | 1×10^{-4} | 1.161×10^{-3} | 2×10^{-6} |
| 1:20 | 4.768 | 2×10^{-3} | 1.499×10^{-2} | 2×10^{-5} | 1.3365 | 1×10^{-4} | 2.938×10^{-3} | 4×10^{-6} |
| 1:10 | 9.102 | 3×10^{-3} | 3.085×10^{-2} | 3×10^{-5} | 1.3396 | 1×10^{-4} | 6.054×10^{-3} | 7×10^{-6} |

Table S1. From left to right: composition of NaCl solutions (mg/ml); NaCl weight percentage (%w/w), NaCl volume fraction (f_{i-NaCl}); NaCl solution refractive index n_{sol} ($\lambda = 588$ nm and $T = 18$ °C); refractive index variation Δn_{sol} (with respect to DIW).

| KCl:H ₂ O (mg/ml) | KCl% (w/w)* | | $f_{i\text{-KCl}}$ (v/v) | | n_{sol} | | Δn_{sol} | |
|---------------------------------|------------------------|--------------------|--------------------------|---------------------|---------------|--|--|--------------------------------------|
| | Mean | STD | Mean | STD | Mean | STD | Mean | STD |
| 0 (DIW) | 0 | / | 0 | / | 1.333594 | 1.6×10^{-5} | 0 | / |
| 1:10⁷ | 0.964×10^{-5} | 3×10^{-8} | 3.759×10^{-8} | 1×10^{-10} | / | / | 5.9×10^{-9} | 6×10^{-10} |
| 1:10⁶ | 0.964×10^{-4} | 3×10^{-7} | 3.759×10^{-7} | 1×10^{-9} | / | / | 5.9×10^{-8} | 6×10^{-9} |
| 1:10⁵ | 0.964×10^{-3} | 2×10^{-6} | 3.759×10^{-6} | 9×10^{-9} | / | / | 5.9×10^{-7} | 6×10^{-8} |
| 1:10⁴ | 0.964×10^{-2} | 2×10^{-5} | 3.759×10^{-5} | 8×10^{-8} | / | / | 5.9×10^{-6} | 6×10^{-7} |
| 1:1000 | 0.963×10^{-1} | 2×10^{-4} | 3.759×10^{-4} | 7×10^{-7} | / | / | 5.9×10^{-5} | 1×10^{-6} |
| 1:100 | 9.581×10^{-1} | 8×10^{-4} | 3.759×10^{-3} | 5×10^{-6} | 1.3342 | 1.0×10^{-4} | 0.559×10^{-3} | 2×10^{-6} |
| 1:50 | 1.963 | 1×10^{-3} | 7.751×10^{-3} | 8×10^{-6} | 1.3347 | 1.0×10^{-4} | 1.152×10^{-3} | 2×10^{-6} |
| 1:20 | 4.768 | 2×10^{-3} | 1.878×10^{-2} | 2×10^{-5} | 1.3364 | 1.0×10^{-4} | 2.794×10^{-3} | 3×10^{-6} |
| 1:10 | 9.103 | 3×10^{-3} | 3.759×10^{-2} | 3×10^{-5} | 1.3392 | 1.0×10^{-4} | 5.596×10^{-3} | 7×10^{-6} |

Table S2. From left to right: composition of KCl solutions (mg/ml); KCl weight percentage (%w/w), KCl volume fraction ($f_{i\text{-NaCl}}$); KCl solution refractive index n_{sol} ($\lambda = 588$ nm and $T = 18$ °C); refractive index variation Δn_{sol} (with respect to DIW).

concentrations down to 1% w/w, both for NaCl and KCl solutions. Δn_{sol} values at concentrations lower than 1% w/w are then calculated exploiting the linear dependency between NaCl (KCl) concentration (C_{sol}) and refractive index (n_{sol})⁴ of the solution, through estimation of the refractive index increment $d\Delta n_{sol}/dC_{sol}$ that is usually calculated for differential refractometers⁵. In Figure S1a and S1c the Δn_{sol} values calculated through the Monte Carlo analysis down to a concentration of 1% w/w are plotted against the weight fraction (in percent), both for NaCl and KCl solutions, from which it is apparent the linear relationship between Δn_{sol} and C_{sol} . By best-fitting the data in Figure S1a and S1c using a linear regression a refractive index increment $d\Delta n_{sol}/dC_{sol} = 6.5 \pm 0.1 \times 10^{-4}$ RIU/%NaCl w/w and $d\Delta n_{sol}/dC_{sol} = 6.08 \pm 0.06 \times 10^{-6}$ RIU/%KCl w/w is estimated, which is used to calculate Δn_{sol} values of NaCl and KCl solutions at concentrations below 1% w/w, i.e. from 10^{-1} to 10^{-5} % w/w (see Tables S1 and S2 for NaCl and KCl, respectively).

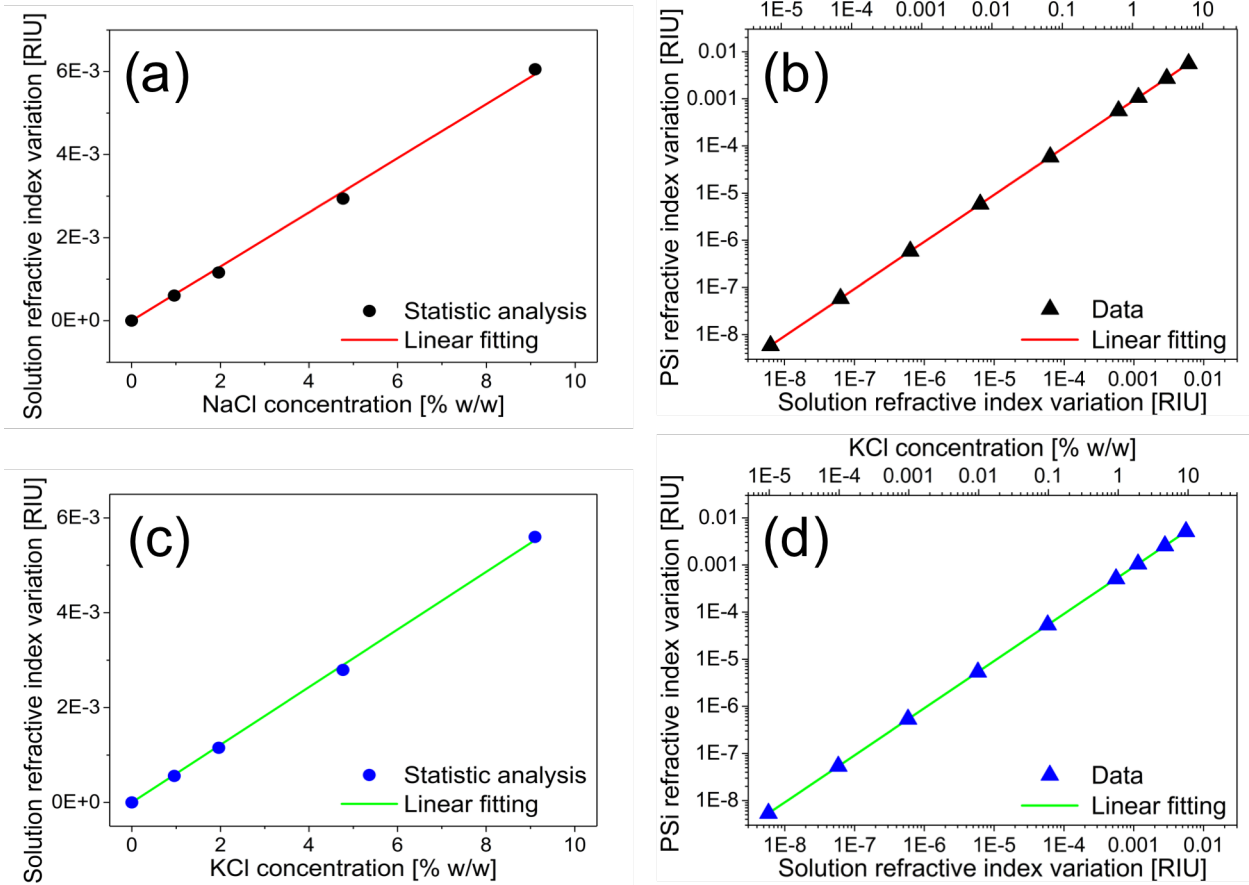


Figure S1. a) Linear relationship between refractive index variation Δn_{sol} (with respect to DIW) and NaCl concentration, C_{sol} , up to 1% w/w NaCl. b) Linear relationship between effective refractive index of the PSi interferometer, n_{eff} , upon infiltration with NaCl solutions at different concentrations and refractive index variation Δn_{sol} (bottom x -axis) at different NaCl concentrations (top x -axis). c) Same as in a) for KCl. d) Same as in b) for KCl.

Section 3. Experimental optofluidic setup

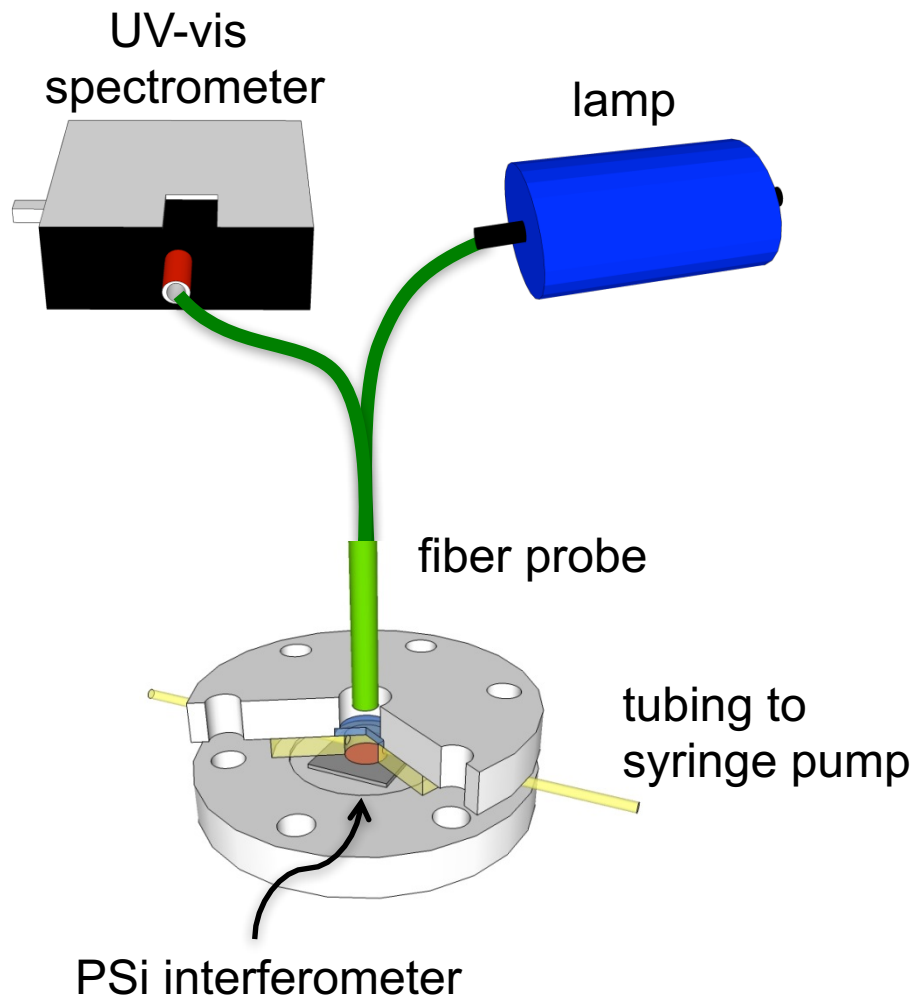


Figure S2. Optofluidic experimental setup for reflection measurements on PSi interferometers, consisting of a home-made plexiglas flow-cell system securing the PSi interferometers, provided with a chamber with volume of 100 μL and a transparent sapphire windows on top sealing the chamber. A UV-VIS spectrometer (USB2000-VIS-NIR-ES) purchased from Ocean Optics (USA) is used to acquire reflectance spectra of the PSi interferometers through the use of a bifurcated fiber-optic probe (QR200-7-VIS-BX) connected to one arm with a halogen lamp source (HL-2000).

Section 4. IAW reflectance spectroscopy calculation routine

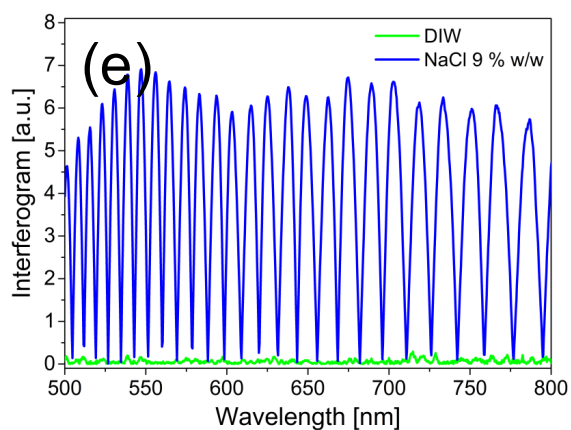
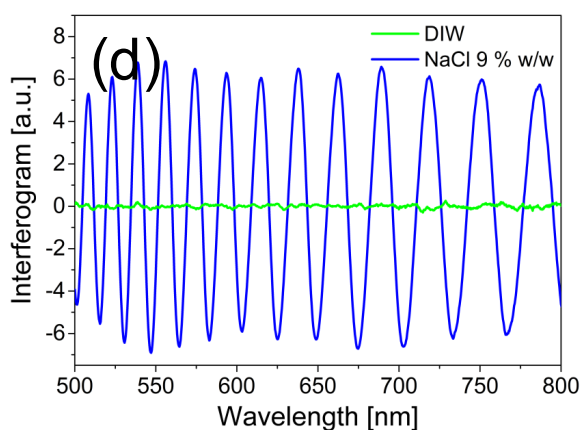
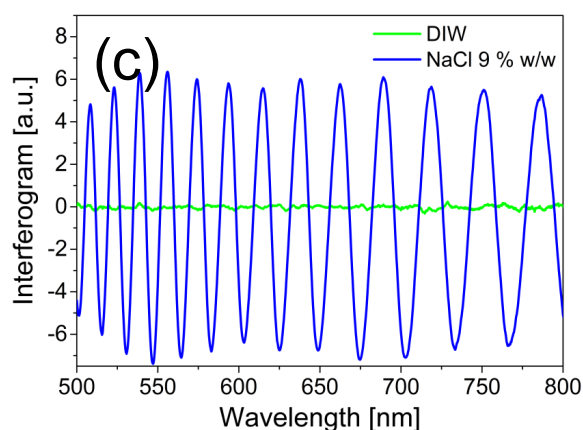
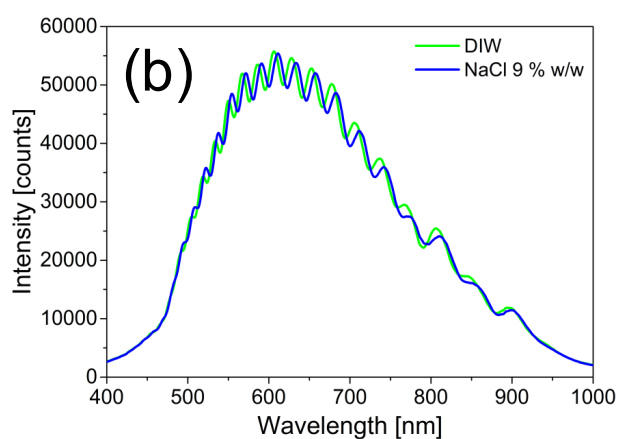
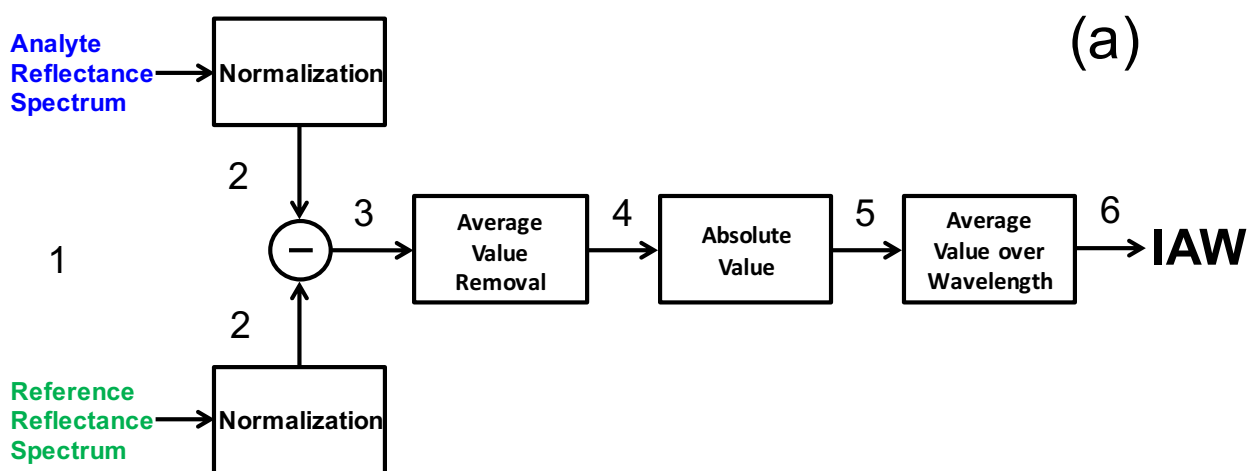


Figure S3. a) Flow-chart of Interferogram Average over Wavelength (IAW) reflectance spectroscopy analysis with main steps highlighted: (step 1) acquisition of reflection spectra; (step 2) extraction of reflectance spectra through normalization with respect to a reference mirror; (step 3) spectral interferogram calculation by subtraction of analyte and reference reflectance spectra; (step 4) removal of the average value of spectral interferogram; (step 5) application of the absolute value function to the spectral interferograms obtained in step 4; (step 6) calculation of the IAW signal as the average value over the wavelength range of interest of the interferogram obtained in step 5. b-d) Application of the routine to calculation of IAW value for DIW (reference solution) and for 9% w/w NaCl

solution: b) experimental reflection spectra acquired on oxidized PSi interferometers in DIW before (green trace) and after (blue trace) infiltration of 9% w/w NaCl solution (step 1 in a); c) spectral interferogram calculation for DIW (green trace) and 9% w/w NaCl solution (blue trace) (step 3 in a); d) removal of the average value of the spectral interferograms calculated in c) (step 4 in a); e) application of the absolute-value function to the spectral interferograms calculated in d) (step 5 in a). The IAW values for DIW and 9% w/w NaCl solution are eventually calculated as the average values of the interferograms in e) over the wavelength range 500-800 nm.

Section 5. Theoretical modeling of PSi interferometers for monitoring bulk refractive index variation of the solution infiltrating the pores using IAW reflectance spectroscopy

PSi interferometers are modeled as a two-components medium composed of a partially oxidized silicon skeleton and of a medium, either gas (e.g. air) or liquid (e.g. DIW), filling the pores. The effective refractive index n_{eff} of an oxidized PSi interferometer filled with a given medium is evaluated by using the Bruggeman effective medium approximation⁶⁻⁸, once porosity P of the PSi layer and refractive indices of both skeleton $n_{skeleton}$ and filling medium n_{fill} are known:

$$P \frac{n_{fill}^2 - n_{eff}^2}{n_{fill}^2 + 2n_{eff}^2} + (1 - P) \frac{n_{skeleton}^2 - n_{eff}^2}{n_{skeleton}^2 + 2n_{eff}^2} = 0 \quad [1]$$

Any change in the value of the refractive index n_{fill} of the filling medium (e.g. through dissolution of different NaCl concentrations in DIW) produces a corresponding change in the value of the PSi layer refractive index n_{eff} and, in turn, a change in the reflectance spectrum of the PSi interferometer.

A first-order theoretical model of a PSi interferometer analyzed using IAW reflectance spectroscopy aimed at evaluating the effect on the *IAW* signal of bulk refractive index variation of the medium infiltrating the pores is analytically implemented under the following hypotheses: 1) light absorption by both PSi skeleton and filling medium is considered to be negligible (imaginary part of refractive indices is negligible over the wavelength range of investigation and, in turn, refractive indices can be considered to be real numbers); 2) wavelength dependence of refractive indices of both silicon and filling medium is considered to be negligible (real part of refractive indices is constant over the wavelength range of investigation); 3) variation of the refractive index of the medium infiltrating the PSi interferometer is significantly smaller than the refractive index value of the reference filling

medium (i.e. DIW, in this work), that is $\Delta n_{fill} \ll n_{fill0}$, being n_{fill0} the refractive index value of the reference medium (i.e. DIW in this work).

Under these assumptions, the typical reflectance spectrum of PSi interferometers can be calculated as⁹:

$$R(\lambda) = \rho_a^2 + \rho_b^2 + 2\rho_a\rho_b \cos(\delta_{layer}) \quad [2]$$

Where ρ_a and ρ_b are index contrast at the filling medium–PSi and PSi–bulk silicon interfaces, respectively:

$$\rho_a = \frac{n_{fill} - n_{eff}}{n_{fill} + n_{eff}},$$

$$\rho_b = \frac{n_{eff} - n_{Si}}{n_{eff} + n_{Si}},$$

The first two terms in Eq. 2, namely ρ_a^2 and ρ_b^2 , represent the intensity contributions of reflected light at filling medium–PSi interferometer and PSi interferometer–bulk silicon interfaces, respectively; the third term takes into account constructive and destructive interference of light reflected at the two interfaces above mentioned, where δ_{PSi} represents the phase delay of the interfering light beams reflected at the two interfaces:

$$\delta_{PSi} = 2 \frac{2\pi n_{eff} d}{\lambda},$$

Where d is the PSi thickness and λ the wavelength.

Eq. 2 is used to calculate theoretical reflectance spectra of PSi interferometers infiltrated with either DIW (reference spectrum) or with DIW containing NaCl at the concentrations used in this work. Subtraction of the generic reflection spectrum after NaCl infiltration R from the reference reflection spectrum in DIW R_0 leads to the following theoretical expression of the interferogram:

$$R - R_0 = (\rho_a^2 - \rho_{a0}^2) + (\rho_b^2 - \rho_{b0}^2) + 2[\rho_a\rho_b \cos(\delta_{PSi}) - \rho_{a0}\rho_{b0} \cos(\delta_{PSi0})] \quad [3]$$

The first two terms in Eq. 3 are constant over wavelength (assumption 1), while the third term represents an oscillating wavelength-dependent signal with mean value close to zero (the mean value is exactly zero when wavelength range over which it is evaluated is an integer multiple of its period).

For small variation of the refractive index values with respect to their reference values, Eq. 3 can be simplified as follows (assumption 3):

$$R - R_0 \cong -8\rho_{a0}\rho_{b0}\pi\Delta n_{eff} \frac{d}{\lambda} \sin\left(4\pi n_{eff0} \frac{d}{\lambda}\right) \quad [4]$$

The IAW value is eventually calculated by taking the absolute value of Eq. 4, then calculating the mean value over a sufficiently large wavelength interval centered around λ_0 :

$$IAW = \text{mean}(|R - R_0|) \Big|_{\lambda_1}^{\lambda_2} \cong \frac{16d|\rho_{a0}\rho_{b0}|}{\lambda_0} |\Delta n_{eff}| \quad [5]$$

where the mean value is calculated by assuming that the $1/\lambda$ function is slowly variable within the wavelength interval $[\lambda_1; \lambda_2]$ and it can be approximated with a constant term $1/\lambda_0$.

Equation 5 highlights a linear relationship between IAW value and PSi refractive index variation Δn_{eff} value, at least under operating conditions for which all the assumptions made hold true. According to Eq. 5, PSi interferometers have theoretical sensitivity to bulk refractive index variation of the solution infiltrating the pores $\frac{16d|\rho_{a0}\rho_{b0}|}{\lambda_0}$, which is proportional to both index contrast ρ_a and ρ_b , and to PSi thickness d , and is inversely proportional to the central wavelength λ_0 of the wavelength interval selected for mean value calculation.

Both porosity P and $n_{skeleton}$ values of oxidized PSi interferometers are estimated by solving the Bruggeman effective medium approximation (Eq. 1) for the two cases of pores filled with either air or DIW:

$$P \frac{n_{Air}^2 - n_{effAir}^2}{n_{Air}^2 + 2n_{effAir}^2} + (1 - P) \frac{n_{skeleton}^2 - n_{effAir}^2}{n_{skeleton}^2 + 2n_{effAir}^2} = 0 \quad [6]$$

$$P \frac{n_{DIW}^2 - n_{effDIW}^2}{n_{DIW}^2 + 2n_{effDIW}^2} + (1 - P) \frac{n_{skeleton}^2 - n_{effDIW}^2}{n_{skeleton}^2 + 2n_{effDIW}^2} = 0 \quad [7]$$

with $n_{Air} = 1$ and $n_{DIW} = 1.333594$. The refractive indices of the PSi interferometers in air n_{effAir} and with DIW infiltrating the pores n_{effDIW} are evaluated from EOT values, namely EOT_{Air} and EOT_{DIW} , obtained from FFT amplitude spectra of PSi reflectance spectra acquired in air and with DIW:

$$n_{effAir} = \frac{EOT_{Air}}{2d} = 1.503416,$$

$$n_{effDIW} = \frac{EOT_{DIW}}{2d} = 1.828572,$$

Where $d = 4669.8$ nm is the thickness of the PSi layer. By solving the system of equations 6 and 7 for both P and $n_{skeleton}$ the following values for $P = 0.734$ and $n_{skeleton} = 3.710463$ are obtained. For the refractive index of bulk silicon the following value $n_{Si} = 3.975$ at 588 nm is used¹⁰. The lower value of $n_{skeleton}$ with respect to n_{Si} is compatible with partial oxidation of PSi. Once P and $n_{skeleton}$ are known, n_{eff} is calculated for the different tested NaCl solutions using Eq. 1.

A linear relationship is obtained between n_{eff} and NaCl solution refractive index n_{sol} with slope $\alpha=0.9248$ (Figure S1b). Accordingly, Eq. 5 can be rewritten to explicitly highlight the dependence of IAW value on the refractive index variation of the NaCl solution infiltrating the PSi interferometer:

$$IAW \cong \frac{16d|\rho_{a0}\rho_{b0}|}{\lambda_0} \alpha |\Delta n_{sol}| \quad [8]$$

Figure S4b highlights a very good agreement, at least within the range of NaCl concentrations tested in this work, between IAW values obtained through the use of Eq. 2 and through the use of Eq. 8, which validates all assumptions made to obtain Eq. 8 from Eq. 2. A maximum relative error smaller than 2.5 % is achieved, thus confirming the validity of Eq. 8 and all assumptions made to get it, at least within the range of NaCl concentrations used in this work.

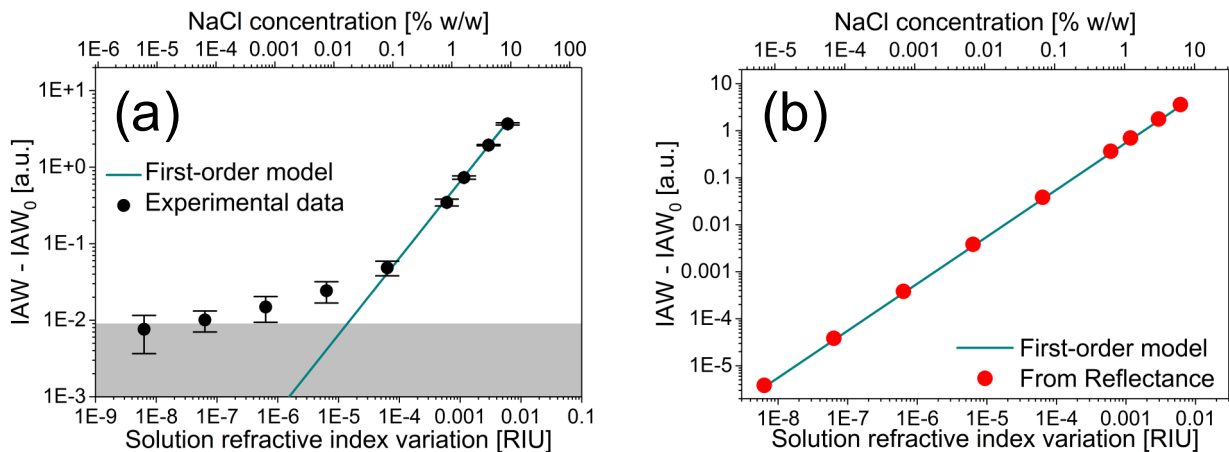


Figure S4. a) Theoretical $IAW - IAW_0$ values calculated through the use of Eq. 8 (solid line) compared to experimental $IAW - IAW_0$ data (solid circle) as a function of bulk refractive index variation Δn_{sol} (bottom x-axis) and NaCl concentration (top x-axis) of the solution infiltrating the pores. A deviation from the theoretical linear trend is recorded at the lower NaCl concentrations. Gray area represents the region within which the $IAW - IAW_0$ signal is lower than $3 \sigma_{IAW_0}$, being σ_{IAW_0} the noise floor

recorded in DIW. b) $I_{AW}-I_{AW_0}$ values obtained using Eq. 2 (red dots) and Eq. 8 (green trace) as a function of bulk refractive index variation Δn_{sol} (bottom x -axis) and NaCl concentration (top x -axis) of the solution infiltrating the pores.

Section 6. Calibration curve of PSi interferometers infiltrated with NaCl aqueous solutions at different concentrations obtained through Fast Fourier Transform (FFT) reflectance spectroscopy

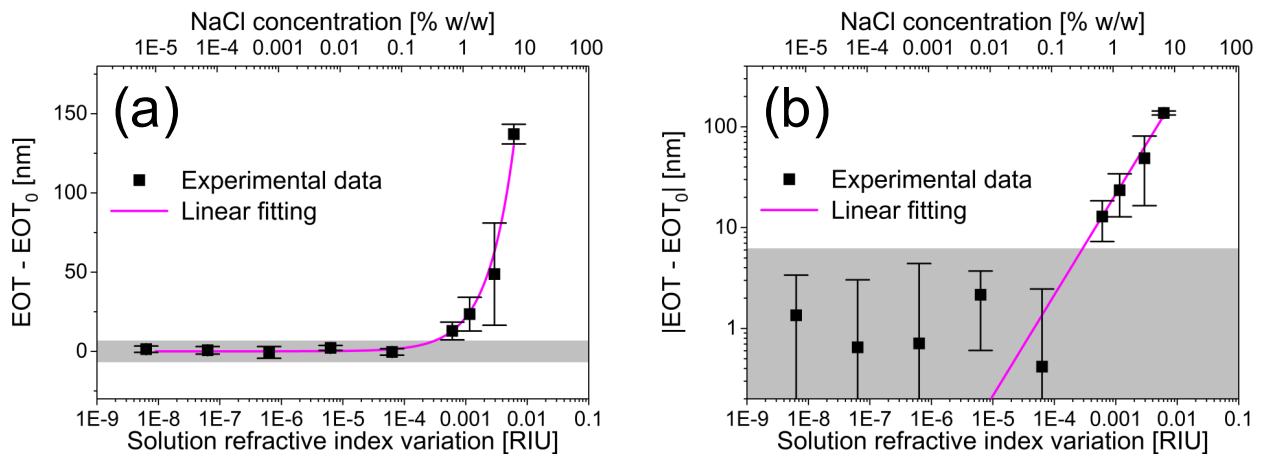


Figure S5. Calibration curve in semi-log scale (a) and log-log scale (b) of $EOT-EOT_0$ signal estimated by FFT reflectance spectroscopy (on the same experimental dataset analyzed using IAW reflectance spectroscopy) as a function of refractive index variation Δn_{sol} (bottom x -axis) and NaCl concentration (top x -axis) of the solution infiltrating the pores. Gray area represents the region within which the $EOT-EOT_0$ signal is lower than $3\sigma_{IAW_0}$, being σ_{IAW_0} the noise floor recorded in DIW. It is apparent that FFT reflectance spectroscopy does not allow the effect of EDL-induced ion surface accumulation on the PSi inner surface to be appreciated.

Reference

- [1] Daimon, M.; Masumura, A. Measurement of the Refractive Index of Distilled Water from the near-Infrared Region to the Ultraviolet Region. *Appl. Opt.* **2007**, *46*, 3811.
- [2] Li, H. H. Refractive Index of Alkali Halides and Its Wavelength and Temperature Derivatives. *J. Phys. Chem. Ref. Data* **1976**, *5*, 329–528.
- [3] Heller, W. Remarks on Refractive Index Mixture Rules. *J. Phys. Chem.* **1965**, *69*, 1123–1129.
- [4] Shippy, B. A.; Burrows, G. H. The determination of potassium and sodium as chloride through the use of the refractometer. *J. Am. Chem. Soc.* **1918**, *40*, 185–187.

- [5] Tumolo, T.; Angnes, L.; Baptista, M. S. Determination of the Refractive Index Increment (dn/dc) of Molecule and Macromolecule Solutions by Surface Plasmon Resonance. *Anal. Biochem.* **2004**, *333*, 273–279.
- [6] Bohren, C. F.; Huffman, D. R. A Potpourri of Particles. In *Absorption and Scattering of Light by Small Particles*; Wiley-VCH Verlag GmbH, 1998; pp. 181–223.
- [7] Pickering, C.; Beale, M. I. J.; Robbins, D. J.; Pearson, P. J.; Greef, R. Optical Properties of Porous Silicon Films. *Thin Solid Films* **1985**, *125*, 157–163.
- [8] Greef, C. P. and M. I. J. B. and D. J. R. and P. J. P. and R. Optical Studies of the Structure of Porous Silicon Films Formed in P-Type Degenerate and Non-Degenerate Silicon. *J. Phys. C Solid State Phys.* **1984**, *17*, 6535.
- [9] Sailor, M. J. Chemistry of Porous Silicon. In *Porous Silicon in Practice*; Wiley-VCH Verlag GmbH & Co. KGaA, 2011; pp. 189–227.
- [10] Palik, E.; *Handbook of Optical Constants of Solids Vol I*, Academic Press, Orlando, 1985, pp 577–580.